Microbial Biotechnology

WILEY

MICROBIAL BIOTECHNOLOGY Open Access

RESEARCH ARTICLE OPEN ACCESS

Disarming the Pathogenicity of Methicillin-Resistant *Staphylococcus aureus* via Osmundacetone-Mediated Inhibition of Sortase A

Rong Wang[1] | Chunhui Zhao[1] | Dongbin Guo[1] | Yueying Wang[1] | Luanbiao Sun[2] | Xinyao Liu[1] | Yun Sun[1] | Da Liu[1] | Jiyu Guan[3] | Li Wang[1] | Bingmei Wang[1]

[1]Changchun University of Chinese Medicine, Changchun, China | [2]China-Japan Union Hospital of Jilin University, Jilin University, Changchun, China | [3]State Key·Laboratory for Diagnosis and Treatment of Severe Zoonotic Infectious Diseases, Key Laboratory for Zoonosis Research of the Ministry of Education, Jilin University Changchun, China

Correspondence: Li Wang (liwang1006@126.com) | Bingmei Wang (bingmeiwang1970@163.com)

Received: 10 October 2024 | **Revised:** 7 January 2025 | **Accepted:** 13 February 2025

Funding: This work was supported by Jilin Provincial Traditional Chinese Medicine Science and Technology Program (2024069), Jilin Provincial Science and Technology Development Plan, (YDZJ2024011l3ZYTS, YDZJ202501ZYTS177).

Keywords: antivirulence | methicillin-resistant Staphylococcus aureus | osmundacetone | sortase A

ABSTRACT

Methicillin-resistant *Staphylococcus aureus* (MRSA) is a major global health threat due to its resistance to multiple antibiotics, making conventional treatments ineffective. The rise in antibiotic resistance highlights the urgent need for new therapies. Sortase A (SrtA), a key virulence factor in *Staphylococcus aureus* (*S. aureus*), facilitates bacterial adhesion and infection by anchoring surface proteins to host cells, making it a promising drug target. In this study, we investigated the potential of osmundacetone (OSC), a natural compound from Osmundae Rhizoma, as an SrtA inhibitor. Using fluorescence resonance energy transfer (FRET), OSC was found to inhibit SrtA with an IC_{50} of 1.29 μg/mL (7.24 μM). Further in vitro assays confirmed the effectiveness of OSC in inhibiting SrtA-mediated bacterial adhesion, invasion and biofilm formation. Fluorescence quenching and molecular docking pinpointed the binding site of OSC on SrtA. In vivo, OSC improved survival rates in MRSA-infected mice and *Galleria mellonella* (*G. mellonella)* while reducing bacterial loads in infected tissues. These results suggest OSC as a promising candidate for anti-MRSA therapies.

1 | Introduction

Staphylococcus aureus (*S. aureus*), a pervasive commensal bacterium (Wertheim et al. 2005), frequently colonises the nasal mucosa and skin surface (Hanselman et al. 2009) of its hosts, harbouring an innocuous presence in approximately 20%–30% of healthy individuals (González-García et al. 2022). This bacterium, under ordinary circumstances, coexists with its human host without incident. However, when the integrity of the skin or mucosal barrier is compromised, *S. aureus* transitions from a harmless bystander to a potent pathogen (Wilson et al. 2011). It can infiltrate underlying tissues or invade the bloodstream, precipitating a range of serious infectious diseases (Cheung et al. 2021), such as cellulitis, pneumonia, endocarditis and the potentially fatal conditions of bacteremia and sepsis (Nagarajan et al. 2024; Yarovoy et al. 2019). Moreover, individuals with compromised immune systems or those reliant on invasive medical devices are particularly vulnerable to these infections (Howden et al. 2023; Lowy 1998; Tong et al. 2015).

Rong Wang and Chunhui Zhao contributed equally to this study.

Traditionally, antibiotics have been the cornerstone of therapy against *S. aureus* infections (Liu et al. 2011), exerting their effects through interactions with bacterial DNA, RNA, proteins, or cell wall components to achieve bactericidal or bacteriostatic outcomes (Gatta et al. 2020; Gao and Zhang 2021). Nevertheless, the landscape of bacterial resistance has been dramatically altered by the production of antibiotic-neutralising enzymes by bacteria, along with the widespread increase in antibiotic use in clinical settings (Chan et al. 2013). This has led to the emergence of formidable, multidrug-resistant strains, notably methicillin-resistant *Staphylococcus aureus* (MRSA) (Ahmad-Mansour et al. 2021), which is now the principal agent of hospital- and community-acquired infections worldwide (Turner et al. 2019). Alarmingly, projections indicate that by 2050 (Christaki et al. 2020), deaths due to antibiotic-resistant infections could surpass those associated with cancer. This resistance is driven principally by the *mecA* gene (Ito et al. 1999), which encodes a modified penicillin-binding protein (PBP2a) that renders bacteria impervious to β-lactam (Chambers and Deleo 2009) antibiotics (Enright et al. 2000). Furthermore, the rapid evolution of antibiotic resistance in *S. aureus* has enabled the bacterium to also resist other classes of antibiotics, including vancomycin and macrolides (Ito et al. 1999; Monecke et al. 2011), compounding the challenge of effective treatment and underscoring the urgent need for innovative therapeutic approaches.

In response to this escalating threat, the strategy of antivirulence factor therapy has gained traction. This approach targets the virulence factors of *S. aureus*—bacterially derived molecules such as hemolysin (Hla) (Lakhundi and Zhang 2018), multiple gene regulator A (MgrA), caseinolytic protease P (ClpP) (Song et al. 2022), sortase A (SrtA) and coagulase—which are intimately linked to its pathogenicity (Beceiro et al. 2013; Jenul and Horswill 2019; Tilouche et al. 2021). These factors facilitate bacterial infection and proliferation within the host (Nisar et al. 2021; Pan et al. 2020). By inhibiting these virulence factors, the strategy aims to attenuate the ability of pathogens to cause disease, rendering them more vulnerable to eradication by the immune system of the host. This method aims to diminish the selective pressure that drives the evolution of resistance, offering a sustainable path forward in managing bacterial infections.

Central to the virulence of *S. aureus* is the enzyme SrtA, which anchors over 20 different cell wall-anchored (CWA) (Foster 2019) proteins to the bacterial surface. These proteins, which include fibrinogen-binding proteins (FnbA and FnbB), clumping factors (ClfA and ClfB) (Ganesh et al. 2011; Xiang et al. 2012) and serine-aspartate repeat proteins (SdrC, SdrD and SdrE) (Askarian et al. 2017), play critical roles in bacterial colonisation, host invasion and immune evasion. The absence of SrtA in *S. aureus* results in significantly reduced virulence (Mazmanian et al. 2000; Weiss et al. 2004), suggesting that inhibition of this enzyme could be a potent therapeutic strategy. Importantly, targeting SrtA does not impair bacterial viability directly, nor does it exert selective pressure on human cells, thus mitigating the risk of developing resistant strains (Cascioferro, et al. 2014; Zecconi and Scali 2013). Additionally, SrtA is crucial for the formation of biofilms, a major factor in chronic infections. Therefore, therapies that inhibit SrtA could not only curb bacterial virulence but also impede biofilm development (Cascioferro, et al. 2014), substantially alleviating the severity of infections (Maresso and Schneewind 2008).

Given its unique extracellular location and absence of homologous structures in eukaryotic cells (Ha et al. 2020), SrtA represents an ideal target for the development of novel antivirulence agents designed to combat the formidable challenges posed by *S. aureus* infections. This innovative approach holds promise for the future, where the threat of antibiotic resistance can be effectively managed, safeguarding global health outcomes.

Currently, several SrtA inhibitors, including natural compounds, small peptides and other related substances, have been identified as having significant therapeutic potential against *S. aureus* infections in vivo (Cascioferro, et al. 2014; Maresso and Schneewind 2008; Wallock-Richards et al. 2015). With the continuous emergence of new drug development strategies, the unique value and importance of natural products have become increasingly prominent. Osmundacetone (OSC), a natural compound, is derived from the rhizome of Osmundae Rhizoma (Trinh et al. 2021). The rhizome of *Osmunda japonica*, referred to as 'Osmundae Rhizomathe' or 'Guan-Zhong' in Chinese (Zhu and Woerdenbag 1995), has various effects, such as anti-inflammatory effects, diuretic effects, skin protection and prevention of gastrointestinal bleeding, and plays a significant role in traditional Chinese medicine (TCM) (Marshall 2020). OSC is known for its neuroprotective and antiapoptotic effects (Béni et al. 2021). Additionally, OSC exhibits a range of activities, including DPPH scavenging, antioxidant effects and the inhibition of immune cytokine and tumour necrosis factor production (Kowalska et al. 2021).

In this study, the inhibitory activity of OSC against *S. aureus* SrtA at a low IC_{50} was screened via FRET technology. These results demonstrated that OSC effectively inhibited SrtA, significantly reducing the pathogenicity of MRSA. Additionally, the in vivo therapeutic efficacy of OSC was evaluated. Given the critical role of SrtA in *S. aureus* infections, our findings support OSC as a promising therapeutic agent with broad potential applications in the treatment of MRSA infections.

2 | Materials and Methods

2.1 | Reagents and Materials

S. aureus USA300 (ATCC BAA-1717) was obtained from the American Type Culture Collection (ATCC) in Manassas, Virginia, USA. The *S. aureus* USA300 strain lacking the SrtA gene *(ΔsrtA) srtA*-deficient strain (Δ*srtA*) and the *Escherichia coli* (*E. coli*) BL21 (DE3) pET28a-*srtA* ΔN59 (Deng et al. 2014) strains used in this study were obtained from our laboratory and were cultured overnight in brain–heart infusion (BHI, Qingdao, China) or Luria Bertani (LB, Qingdao, China) broth in an incubator with shaking at 220 rpm at 37°C unless otherwise indicated. Osmundacetone was sourced from Letian Mei Biology Co. Ltd. and was obtained from Chengdu, China (Figure S1). It is a light yellow powder that was dissolved in DMSO to prepare a 10 mg/mL stock solution before use. This stock solution was then diluted to the desired concentrations

for experimental applications. The fluorescent substrate peptide Abz-LPATG-Dap (Dnp)-NH_2 was purchased from LifeTein LLC (Beijing, China). Human non–small-cell lung cancer cells (A549 cells) were grown in complete medium containing 5% foetal bovine serum and 1% streptomycin and penicillin and were grown in 5% CO_2 as well as in a 37°C cell culture incubator for 24 h.

2.2 | Plasmid Construction

The pET28a prokaryotic expression vector was utilised for cloning in this experiment. The DNA sequence that encodes the *srtA* gene was amplified via PCR with *S. aureus* USA300 genomic DNA as a template. The PCR products were then digested with *XhoI* and *BamHI* (NEB, China) and cloned and inserted into the same locus of pET28a. After the sequence was confirmed via DNA sequencing, the pET28a-*srtA* ΔN59 plasmid was obtained. A QuikChange Targeted Mutagenesis Kit (Stratagene, USA) was used to target G167A SrtA, V168A SrtA, L175A SrtA and Q178A SrtA in Table S2.

2.3 | Purification of SrtA and Its Mutants

The recombinant plasmid pET28a-*srtA* was incubated with *E. coli* BL21 (DE3) in LB media at 220 rpm and 37°C with shaking until the concentration reached the range of 8×10^7–8×10^8 CFU/mL. Isopropyl-β-d-thiogalactopyranoside (IPTG, BioWorks Biotech, China) was then added to the suspension to a concentration of 0.5 mM, which was subsequently incubated overnight at 180 rpm and 18°C with shaking to induce the expression of the SrtA protein. The bacteria were collected by centrifugation at 4°C, the supernatant was discarded, and the bacteria were resuspended in reaction buffer (50 mM Tris base, 150 mM NaCl, 5 mM $CaCl_2$, pH 7.4; Beyotime, China) before being sonicated. After the cells were disrupted, the supernatant was collected by centrifugation at low temperature. The proteins were purified via an Ni-NTA system (Beyotime, China). The heterogeneous proteins were eluted by adding 50 mM imidazole, while the SrtA proteins were sequentially eluted with 100, 200, and 400 mM imidazole, and the purification results are shown in Figure S2. The mutant proteins were purified following the same protocol.

2.4 | Screening of SrtA Inhibitors

FRET was utilised to screen for SrtA inhibitors, leveraging the ability of *srtA* ΔN59 to identify and cleave LPXTG motifs tagged with fluorescent and quenching groups at both ends. This process yielded the products Abz-LPAT-Gly_3 and G-dnp, facilitating the transfer of fluorescence. The process is depicted in Figure 1a. A FRET assay was used to detect the activity of the purified SrtA protein. A final volume of 100 μL of a mixture containing SrtA reaction buffer, purified SrtA protein and various concentrations of small molecule compounds was added to a black 96-well plate and incubated for 30 min at 37°C. The fluorescent substrate peptide Abz-LPATG-Dap (Dnp)-NH_2 was subsequently incubated at the same temperature for 20 min. Negative controls were included in wells containing all the components except for the SrtA protein. The fluorescence intensity was measured via an enzyme marker (TECAN, M1000, Switzerland) at 420 nm for emission and 309 nm for excitation. IC_{50} values were calculated with GraphPad Prism 8.0 software.

2.5 | Reversible Inhibition Assay of SrtA

The SrtA protein was added to the reaction buffer at a final concentration of 100 μg/mL, along with the 10-fold IC_{50} concentration of OSC. The mixture was then incubated for 1 h at 37°C, protected from light and subsequently diluted 100-fold by the addition of 9.9 mL of reaction buffer. Following the final addition of 10 μL of the fluorescent substrate peptide Abz-LPATG-Dap (Dnp)-NH_2, the fluorescence intensity was measured at 309 nm excitation and 420 nm emission wavelengths using an enzyme marker. The degree of reversible inhibition was calculated from the measured values.

2.6 | Determination of the Minimum Inhibitory Concentration (MIC) and Growth Curve

In accordance with the CLSI guidelines (Humphries et al. 2021), the MIC of OSC was determined via the microbroth dilution method to evaluate its antimicrobial activity, which was performed as follows: using tryptic soy broth (TSB, HopeBio, China), *S. aureus* was recovered overnight, inoculated the next day at a ratio of 1:100 in cation-adjusted Mueller–Hinton broth (CAMHB, Qingdao, China) and incubated at 37°C until a concentration of 8×10^7–8×10^8 CFU/mL was obtained. Next, the bacterial suspension was diluted 1:1000 in CAMHB and inoculated into sterile 96-well plates, and the concentration of OSC in sterile 96-well plates ranged from 8 to 1024 μg/mL via the multiplicative dilution method. Then, 2 μL of diluted azurophilic dye (5 mg/mL) was added to each well, and the plates were incubated at 37°C in a temperature chamber for 16 h. Finally, the antimicrobial activity of the OSC was evaluated by observing the colour change to assess the antimicrobial effect of the OSC. Moreover, we established a group containing only *S. aureus* USA300 as a positive control group and a group containing only CAMHB medium as a negative control group. USA300 and Δ*srtA* were cultured overnight and transferred in proportion to TSB. They were then incubated until they reached concentrations ranging from 3×10^7 to 3×10^8 CFU/mL. The OD_{600} value was measured every hour via an enzyme marker (Thermo Fisher Scientific, USA), and a growth curve was plotted.

2.7 | MTT Cytotoxicity Assay

The MTT assay was employed to assess the cytotoxicity of the natural products. A549 cells were seeded at a density of 5×10^4 cells per well in a 96-well plate and incubated overnight until they reached 80% confluence. The culture medium was subsequently replaced with Dulbecco's modified Eagle's medium (DMEM) supplemented with various concentrations of OSC (0–64 μg/mL). After a 12-h incubation in the cell culture incubator, 10 μL of MTT (5 mg/mL, Beyotime, China) solution was added to each well, and the mixture was incubated at 37°C for 4 h. Following the removal of the supernatant, 100 μL of

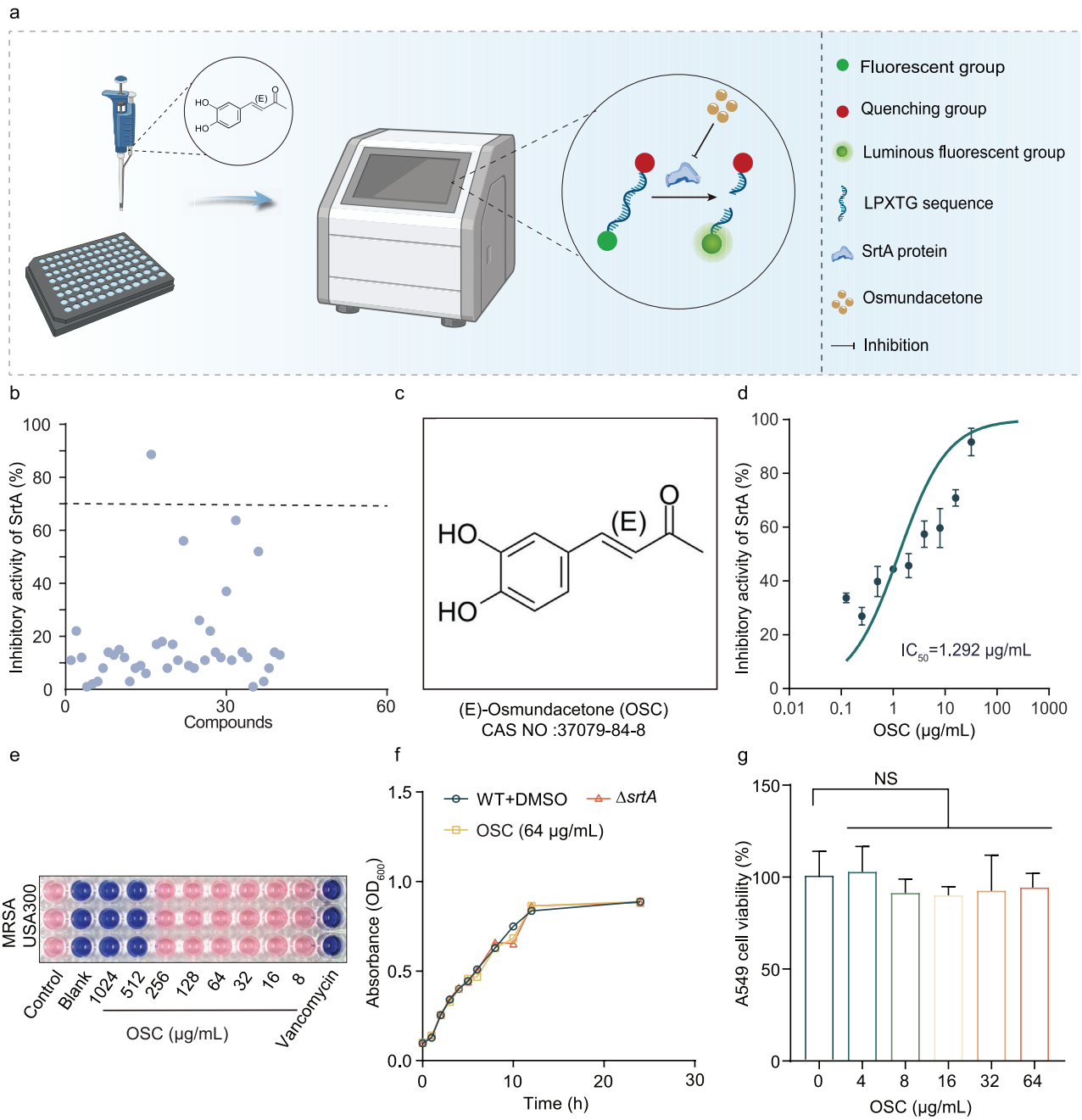

FIGURE 1 | Inhibitory effects of the compound OSC on SrtA activity. (a) FRET experiments were employed to assess the effects of compounds on the ability of SrtA to cleave the LPXTG motif, a process that triggers energy transfer, leading to changes in fluorescence intensity. (b) The inhibitory effects of various compounds on SrtA were explored. Compounds with an inhibition rate exceeding 70% were considered to exhibit potential inhibitory activity. (c) Chemical structural formula of the compound OSC, which has a CAS number of 37079—84—8. (d) Effects of OSC on SrtA activity, with an IC_{50} value of 1.29 μg/mL. (e) MICs of the compound OSC against *S. aureus*. (f) Growth curves of the *S. aureus* USA300 strain and the Δ*srtA* mutant strain after treatment with 64 μg/mL OSC for 24 h. (g) Different concentrations of OSC (0–64 μg/mL) had no effect on the viability of A549 cells.

dimethyl sulfoxide (DMSO) was added to dissolve the formazan crystals in each well. The absorbance of each well at 570 nm was then measured via a microplate reader.

2.8 | Fibrinogen Binding Assay

Fibrinogen (Fn, 20 μg/mL, Yuanye, China) was added to a 96-well plate and incubated overnight at 4°C. The plate was then washed with phosphate-buffered saline (PBS) and incubated with 0.5% bovine serum albumin (BSA) for 2 h. Next, different concentrations of OSC (0–64 μg/mL) were mixed with USA300 bacterial suspensions at a concentration of 6×10^7–6×10^8 CFU/mL, and the mixture was added to a 96-well plate for incubation. The plate was incubated at 37°C for 2 h, washed, fixed and then stained with crystal violet. The plate was eluted with anhydrous ethanol, transferred to a new 96-well plate and detected via a microplate reader (Multiskan

Go, Thermo Fisher, USA). The adhesion rate was calculated on the basis of the absorbance value at 570 nm with GraphPad Prism 8.0 software.

2.9 | Biofilm Formation Assay

S. aureus cultured overnight in BHI medium at 37°C with shaking at 220 rpm, along with Δ*srtA*, will be diluted 1:100 in BHI supplemented with glucose and sodium chloride. The cultures were shaken until a concentration ranging from 3×10^7 to 3×10^8 CFU/mL was reached. Simultaneously, 50 μL of 20% lyophilised rabbit plasma (Xiang et al. 2017) (HopeBio, China) was added to a 96-well plate and incubated overnight at 4°C for coating. The following day, bacterial cultures containing various concentrations of OSC (0–64 μg/mL) were added to a plasma-coated 96-well plate. After incubation at 37°C for 16 h, the supernatant was removed, and the wells were washed with PBS. Crystal violet staining will be performed for 20 min, followed by washing with PBS. Subsequently, 200 μL of anhydrous ethanol was added for elution of the bound dye, and the absorbance at 570 nm was measured via a microplate reader.

2.10 | Confocal Laser Scanning Microscopy (CLSM) Detection of Biofilms

The glycerol bacteria were revived at a 1:100 ratio in BHI medium and incubated overnight on a shaker at 37°C. The next day, the bacteria were inoculated at a 1:100 ratio into BHI. Five hundred microlitres of bacterial suspension were inoculated into a six-well plate coated with freeze-dried rabbit plasma and incubated at 37°C for 24 h to form a complete biofilm. The biofilms were treated with different concentrations of OSC and PBS. The mixture was incubated at 37°C for 24 h. After incubation, the supernatant was removed, and the biofilms at the bottom were washed three times with PBS (pH 7.4). The samples were stained with SYTO-9 (Yuanye, China) at room temperature for 30 min, and three-dimensional fluorescence images were captured via CLSM (Carl Zeiss, Germany).

2.11 | FITC-IgG-Labelled *S. aureus* Surface Protein A (SpA)

After oscillation cultivation of *S. aureus* at 37°C and 220 rpm until a concentration ranging from 3×10^7 to 3×10^8 CFU/mL was reached, different concentrations of OSC (32–64 μg/mL) were added under the same conditions and cultured until the concentration was within the range of 1×10^8–1×10^9 CFU/mL. The bacterial cells were then collected by centrifugation, washed once with PBS and blocked with 0.3% BSA for 20 min. After centrifugation and another wash with PBS, the bacterial cells were fixed with 4% paraformaldehyde for 20 min. After rinsing with PBS, the cells were resuspended by adding 50 μL of FITC-labelled rabbit anti-sheep immunoglobulin G (IgG) (Proteintech, China) diluted at a ratio of 1:200, and the cells were incubated in the dark for 2 h at room temperature. After incubation, the cells were washed with PBS to eliminate background fluorescence effects and resuspended in PBS, and the fluorescence intensity was measured via flow cytometry (CytoFlex; Beckman Coulter, USA).

2.12 | Invasion Assay

A549 cells were seeded at a density of 1×10^5 cells per well in a 24-well plate and cultured in F-12 K medium containing foetal bovine serum, streptomycin and penicillin for 24 h. Moreover, *S. aureus* suspensions containing different concentrations of OSC were shaken at 37°C and 220 rpm until the concentration was within the range of 1×10^8–1×10^9 CFU/mL, followed by centrifugation to collect bacterial cells, which were subsequently resuspended in F12-K medium. The cells were subsequently infected with *S. aureus* at a concentration of 1×10^5 CFU/mL. Five hundred microliters of the bacterial suspension at the desired concentration were added to each well of the 24-well plate and incubated at 37°C for 2 h. After being washed with PBS, the cells were incubated in F12-K medium containing gentamicin (300 μg/mL) for 1 h to eliminate extracellular *S. aureus*. Following two PBS washes, the cells were lysed with 5% (v/v) Triton X-100 (Sigma–Aldrich, Germany), and the bacterial counts were determined by plating and incubating the bacteria.

2.13 | Live-Dead Cell Experiment

A549 cells were seeded at a density of 5×10^5 cells per well in a 24-well plate and cultured at 37°C with 5% CO_2 until the cell confluence reached 80%–90%. The cells were then washed twice with PBS. *Staphylococcus aureus* was inoculated into TSB medium at a 1:100 ratio and incubated overnight at 37°C with shaking at 220 rpm. After overnight incubation, the bacterial cells were collected via centrifugation. The bacterial pellet was subsequently resuspended in F-12 K media, and the bacterial concentration was adjusted to 1×10^8–1×10^9 CFU/mL. A total of 500 μL of the bacterial suspension containing varying concentrations of OSC (32–64 μg/mL) was added to each well of the 24-well plate. The plate was incubated at 37°C for 5 h, after which the supernatant was discarded. The cells were then stained in the dark for 30 min via the Calcein-AM/PI Live/Dead Cell Viability/Cytotoxicity Assay Kit (Baiyoutian, China) according to the manufacturer's instructions. After staining, the cells were washed twice with PBS and imaged under a fluorescence microscope (Leica Microsystems, Germany).

2.14 | Quantitative Real-Time PCR (RT–qPCR)

Total RNA from *S. aureus* was extracted via the TRIzol method according to the manufacturer's instructions (Rio et al. 2010). The quantity of total RNA was confirmed via ultraviolet spectrophotometry. Purified *S. aureus* RNA was reverse-transcribed into cDNA via Transcriptor First Strand cDNA Synthesis Master Mix (5X) (with gDNA EZeraser) (Beyotime, China) following the manufacturer's protocol. RT–qPCR analysis was performed via Fast Start Universal SYBR Green Master Mix (Roche Molecular Biochemicals, Germany) and the CFX96 Touch Real-Time PCR Detection System (Bio-Rad). The reference gene used in RT–qPCR was *16S RNA*. Each experiment was performed independently and repeated three times. The sequences of the primers used in the real-time PCR experiments are provided in Table S2.

2.15 | Western Blot Analysis

The *S. aureus* was diluted in TSB at a ratio of 1:100 and cultured until the concentration ranged from 3×10^7 to 3×10^8 CFU/mL. Different concentrations of OSC (0–64 μg/mL) were added, and the cultures were oscillated at 37°C until the concentration was within the range of 2×10^8–2×10^9 CFU/mL. The Δ*srtA* group was used as the control group. After the bacterial cells were collected via centrifugation, they were washed once with PBS. Then, lysozyme (0.2 mg/mL) and lysostaphin (0.01 mg/mL) were added, and the mixture was incubated on ice for 30 min for cell lysis. The supernatant was collected after centrifugation, followed by gel electrophoresis. The proteins were then transferred onto a polyvinylidene fluoride (PVDF) membrane, which was blocked with 2.5% skim milk for 2 h. The PVDF membrane was subsequently incubated overnight at 4°C with polyclonal serum antibodies against *S. aureus* SrtA (1:200; the polyclonal anti-SrtA antibody was produced in-house). After the excess proteins were washed away with TBS-T, the PVDF membrane was incubated with horseradish peroxidase (HRP)-conjugated secondary goat anti-rabbit antibody (1:10,000, Beyotime, China) at room temperature for 2 h. Finally, the bands were visualised via ECL Plus (Beyotime, China) for exposure and recording.

2.16 | Fluorescence Quenching Assay

The purified SrtA protein was diluted to a concentration of 500 ng/mL with PBS and added to a black 96-well plate. Various concentrations of OSC (0.1–0.5 μg/mL) were subsequently added and thoroughly mixed. After incubation at room temperature for 10 min, the fluorescence spectrum of the mixture was measured via a fluorescence spectrophotometer. Fluorescence emission spectra in the range of 300–400 nm were recorded, and K_A values were calculated on the basis of previous methods (Papadopoulou et al. 2005).

2.17 | Molecular Docking

Three-dimensional structural data of the SrtA protein were obtained from the PDB database (PDB ID: 1T2P). The three-dimensional structure of the OSC was obtained from PubChem (PubChem ID: 9942292), and ChemBio3D Ultra 12.0 software was used to construct the three-dimensional structure of the SrtA protein. Moreover, ABEE was used to construct the three-dimensional structure of OSC molecular docking simulations via AutoDock Vina 1.57 software, with a configuration of specific parameters for the docking programme: exhaustiveness was set to 8, and manually customised grid coordinates were set as centre_x = −30.329, centre_y = −19.713 and centre_z = −0.456; dimensions were set as size_x = 47.75, size_y = 45.75 and size_z = 46.5, ensuring precise and accurate analysis of molecular interactions. Nonpolar hydrogen atoms were merged, and rotatable bonds were constrained to generate ligand–protein complexes.

2.18 | Protective Effect of OSC on MRSA-Infected *G. mellonella*

To evaluate the potential of OSC in treating MRSA-induced systemic infection in *G. mellonella*, this study established five experimental groups: the WT infection group, the OSC treatment group, the uninfected control group, the Δ*srtA* mutant infection group and the vancomycin treatment group. Each group consisted of 10 larvae. The infection model was created by injecting 10 μL of an MRSA suspension containing 5×10^8 CFU/mL into the distal part of the left foreleg. One hour after injection, the OSC treatment group received 40 mg/kg OSC, whereas the vancomycin treatment group received 40 mg/kg vancomycin. The uninfected control group and the vancomycin treatment group were also subjected to corresponding treatments to ensure experimental rigour. During the experiment, the larvae were kept at a temperature below 37°C. The survival rate of the larvae was recorded every 12 h over a 96 h observation period. Additionally, to assess treatment efficacy, larvae were collected 48 h post infection, sterilised, homogenised and cultured on TSA plates at 37°C for 24 h to quantify the number of colony-forming units. The extent of larval melanisation was also recorded through images to evaluate the severity of infection and the effectiveness of the treatments.

2.19 | Mouse Model of Pneumonia Infection

All animal experiments in this study were conducted in strict accordance with the regulations of the Animal Ethics Committee of Changchun University of Chinese Medicine. Female specific pathogen-free (SPF)-grade C57BL/6J mice, aged 6–8 weeks, were selected as models for pneumonia infection. The mice were acclimatised in a standard laboratory environment for 1 week with free access to food and water. The mice were randomly divided into five groups: the blank control group, WT + DMSO group, WT + OSC group, vancomycin group and Δ*srtA* group. In the survival experiment, eight mice were used per group. *S. aureus* USA300 was diluted 1:100 in TSB and cultured to concentrations ranging from 1×10^8 to 1×10^9 CFU/mL. After centrifugation, the bacterial pellet was washed and resuspended in PBS. The mice were anaesthetised with isoflurane gas and positioned upright, and 30 μL of bacterial suspension (2×10^8 CFU) was introduced into the left nostril to induce natural inhalation, thereby establishing the *S. aureus* pneumonia infection model. Two hours later, the mice in the treatment and infection groups were subcutaneously injected with OSC (40 mg/kg) or an equivalent volume of DMSO, followed by identical dosing every 12 h. Mouse survival was assessed every 12 h, and a survival curve was plotted over 96 h. The statistical significance of differences between the treatment and control groups was assessed via the log-rank test of the survival curves.

In this study, the mice were randomly assigned to each experimental group ($n = 12$) and intranasally infected with *S. aureus* at a concentration of 1×10^8 CFU/30 μL. All the mice subsequently received drug treatment at the same dosage via the same method. Twenty-four hours postinfection, four mice from each group were randomly selected and euthanised via cervical dislocation. Lung tissue samples were aseptically collected, and bacterial colony counts were performed on agar plates to assess the bacterial load in the lungs. Simultaneously, the left lungs of an additional four mice from each group were fixed in 10% formalin, followed by paraffin embedding, haematoxylin–eosin (H&E) staining, or F4/80 staining for histopathological examination under a light microscope. For the remaining four

mice in each group, lung tissues were rapidly excised after euthanasia, and the wet weight (W) was accurately measured. The lung tissues were then dried for 24 h in an oven preset to 65°C to obtain the dry weight (D). The wet–dry weight ratio (W/D ratio) was calculated to determine the lung W/D ratio for each group, which serves as an important indicator for assessing the degree of pulmonary oedema.

2.20 | Flow Cytometric Detection of Inflammatory Markers in Mouse Lung Tissue

To establish a mouse model of pneumonia infection, female C57BL/6J mice 6 to 8 weeks of age were used in this study. The mice were spontaneously inhaled by dropping 30 μL of a bacterial suspension (containing 1×10^8 CFU) into the left nostril to simulate a respiratory infection. Twelve hours after infection, the mice were anaesthetised with 0.5% pentobarbital, and the lung tissues were removed and sectioned. The tissue pieces were digested in a solution containing digestive enzymes for 20 to 30 min at 37°C and filtered through a cell sieve to obtain a single-cell suspension. The cell suspension was centrifuged at 1000 rpm for 10 min, and the supernatant was discarded. An appropriate amount of erythrocyte lysate was then added to lyse the cells on ice for 5 min, followed by the addition of culture medium to complete the lysis process. After centrifugation for another 10 min, the supernatant was discarded, and the cell precipitate was resuspended in blocking solution and blocked on ice for 10 min. After the blocking solution was discarded, the cells were mixed with appropriately diluted PE-labelled anti-mouse/human CD11b antibody (Elabscience, China) and FITC-labelled anti-mouse Ly6G antibody (Elabscience, China) and incubated for 30 min at 4°C in the dark. After incubation, the mixture was washed with buffer and finally resuspended in buffer for flow cytometry analysis.

2.21 | Statistical Analysis

The experimental data of this study were statistically analysed via GraphPad Prism 8.0, and the results are expressed as the means ± standard deviations (means ± SDs) ($n \geq 3$). A significance level of $p < 0.05$ was considered statistically significant. The Kaplan–Meier log-rank test was used to evaluate the statistical significance of differences between the treatment and control groups on the basis of survival curves. Each experiment was conducted with three parallel biological replicates.

3 | Results

3.1 | Identification of OSC as a SrtA Inhibitor

Using a FRET assay, we screened 40 compounds (Table S1) and ultimately identified the compound OSC as an inhibitor of SrtA (Figure 1b,c) because of its significant inhibitory activity at low doses during the initial tests. The results indicated that OSC markedly inhibited SrtA activity in a dose-dependent manner, with an IC_{50} of 1.29 μg/mL (Figure 1d). Although OSC inhibits SrtA, it does not significantly affect the growth rate of *S. aureus* USA300. The results of resazurin staining revealed that the MIC of OSC against *S. aureus* exceeded 512 μg/mL (Figure 1e), indicating a lack of antibacterial activity. Furthermore, OSC did not exert selective pressure on *S. aureus*, as evidenced by the unchanged growth rate of the USA300 strain (Figure 1f).

To determine cytotoxicity, an MTT assay was performed on the A549 cell line. The results revealed no significant deviations in cell viability across different drug concentrations (0–64 μg/mL) (Figure 1g), indicating that OSC has no cytotoxic effects and has few cytotoxic effects. Furthermore, safety in vivo was assessed via a rabbit erythrocyte assay. Notably, concentrations up to 32-fold the IC_{50} value did not induce hemolysis of rabbit erythrocytes (Figure S3).

The collective evidence from these experiments compellingly supports the conclusion that OSC is not acutely toxic in vivo at the tested concentrations. This absence of toxicity underscores the potential for further development of OSC as a pharmaceutical agent for treating *S. aureus* infections.

3.2 | Effect of OSC on *S. aureus* Pathogenicity

We assessed the impact of OSC on the SrtA activity of *S. aureus* through a series of experiments aimed at understanding its role in reducing the pathogenicity of this bacterium. Initially, a fibrinogen binding assay was performed to evaluate the effect of OSC on the adhesion of *S. aureus*. Given that Fibrinogen (Fn) acts as a crucial bridge between the bacterial adhesin fibrinogen-binding protein (Fnbp) and mammalian cell integrins, influencing phagocytosis, our results demonstrated that OSC significantly diminished *S. aureus* adhesion, reducing it to 18.15% at the highest concentration tested (64 μg/mL) (Figure 2a). These findings suggest that the OSC disrupts the interaction with fibronectin, thereby mitigating the virulence of *S. aureus*.

To further explore the complex interplay between *S. aureus* SrtA and host colonisation, particularly in the context of invasive diseases, we investigated the impact of OSC on the invasive potential of *S. aureus* in A549 cells. By utilising green fluorescence-labelled bacteria, invasion assays revealed that OSC treatment markedly reduced the invasion of host cells, especially at the highest dosage (64 μg/mL) (Figure 2b,c). The colony count on the blood agar plate showed the same results (Figure 2d). The role of the SrtA protein extends to the formation of biofilms, which serve as physical barriers that increase bacterial resistance to antibiotics and survival. Crystal violet staining was used to examine the effects of OSC on both nascent and mature *S. aureus* biofilms. We observed a dose-dependent reduction in biofilm formation in response to OSC, with the lowest level of biofilm formation occurring in the Δ*srtA* group (Figure 2e). However, interestingly, changes in the OSC concentration did not influence mature biofilms (Figure S4). Using confocal laser scanning microscopy, we assessed the structural integrity of the *S. aureus* biofilm and discovered that treatment with OSC led to a deterioration in biofilm integrity and thickness, which was particularly evident compared with the robust biofilms of the WT group (Figure 2f,g).

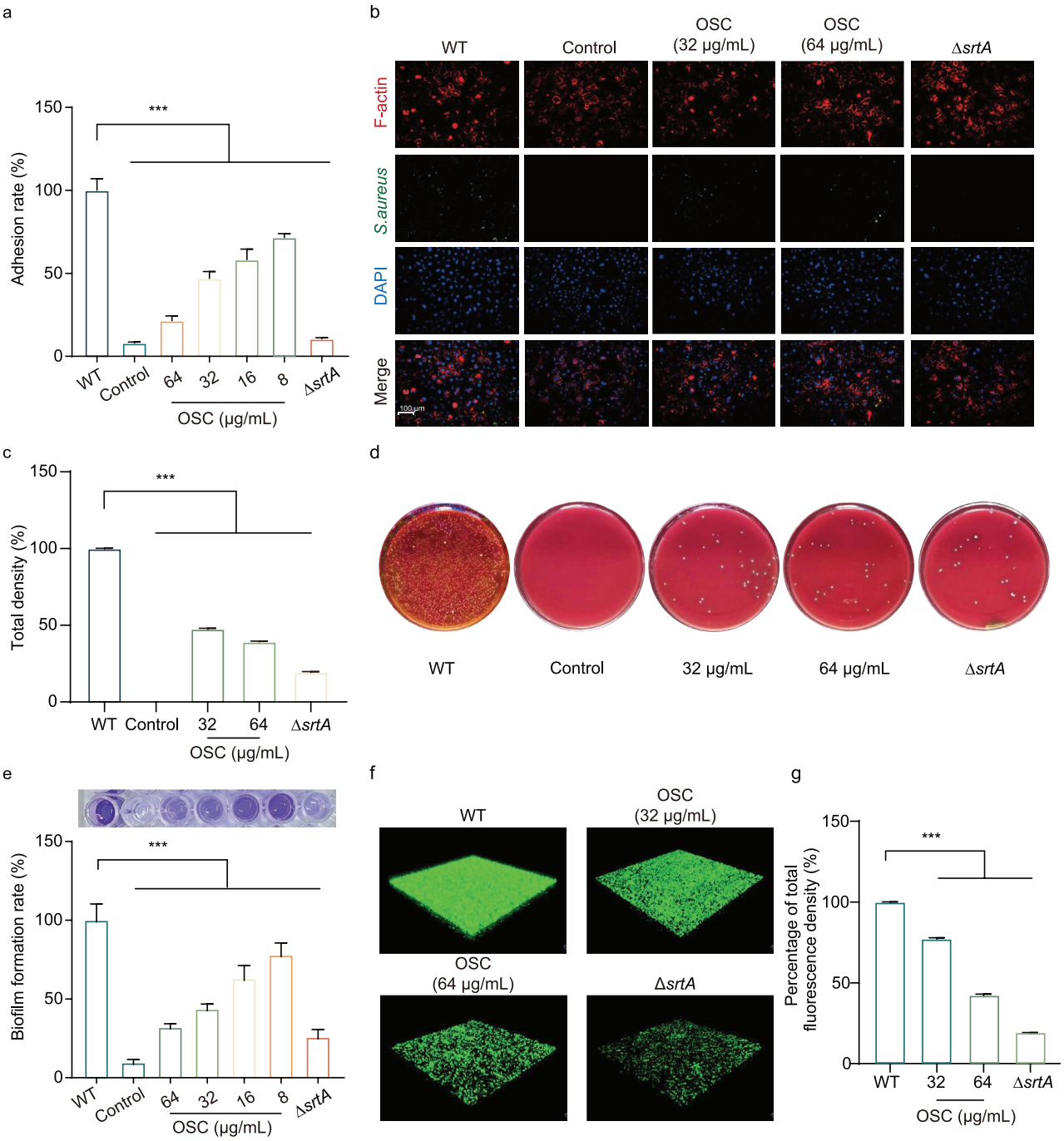

FIGURE 2 | Inhibitory effects of the compound OSC on the SrtA-mediated virulence phenotypes of *S. aureus*. (a) Effects of the compound OSC on the adhesion of *S. aureus* to fibronectin. The results showed that the presence of OSC significantly reduced the adhesion of *S. aureus*. (b) Effects of different concentrations of OSC (32–64 μg/mL) on the internalisation of *S. aureus* into A549 cells. Staining of A549 cells with phalloidin (red) and DAPI (blue) revealed that the number of *S. aureus* internalised into A549 cells decreased as the concentration of OSC increased. (c) Quantitative fluorescence statistics of *S. aureus* invasion into A549 cells confirmed the inhibitory effect of OSC on *S. aureus*. (d) Blood plate colony counting results showing the inhibitory effects of different concentrations of OSC on the internalisation of *S. aureus* into A549 cells, providing quantitative data on the inhibitory effects of OSC. (e, g) The ability of OSC to resist biofilm formation in *S. aureus* was evaluated via crystal violet staining, quantitative fluorescence statistics of the biofilm revealing the destructive effect of OSC on the formation of biofilm. (f) Effects of different concentrations of OSC (0–64 μg/mL) on the formation of *S. aureus* biofilms. The biofilm membranes were stained with the nucleic acid dye SYTO-9 and then reconstructed in three dimensions via confocal laser scanning microscopy (CLSM).

Moreover, the live–dead cell assay confirmed the protective effect of OSC against MRSA-infected A549 cells, which resulted in a significant reduction in bacterial lethality towards host cells (Figure 3a,b).

Additionally, the interaction of SrtA-mediated SpA with the host immune system notably enhances the infectivity of *S. aureus*. Since SpA specifically binds to the Fc region of IgG, we used fluorescence cytometry to determine the effect of OSC on SpA

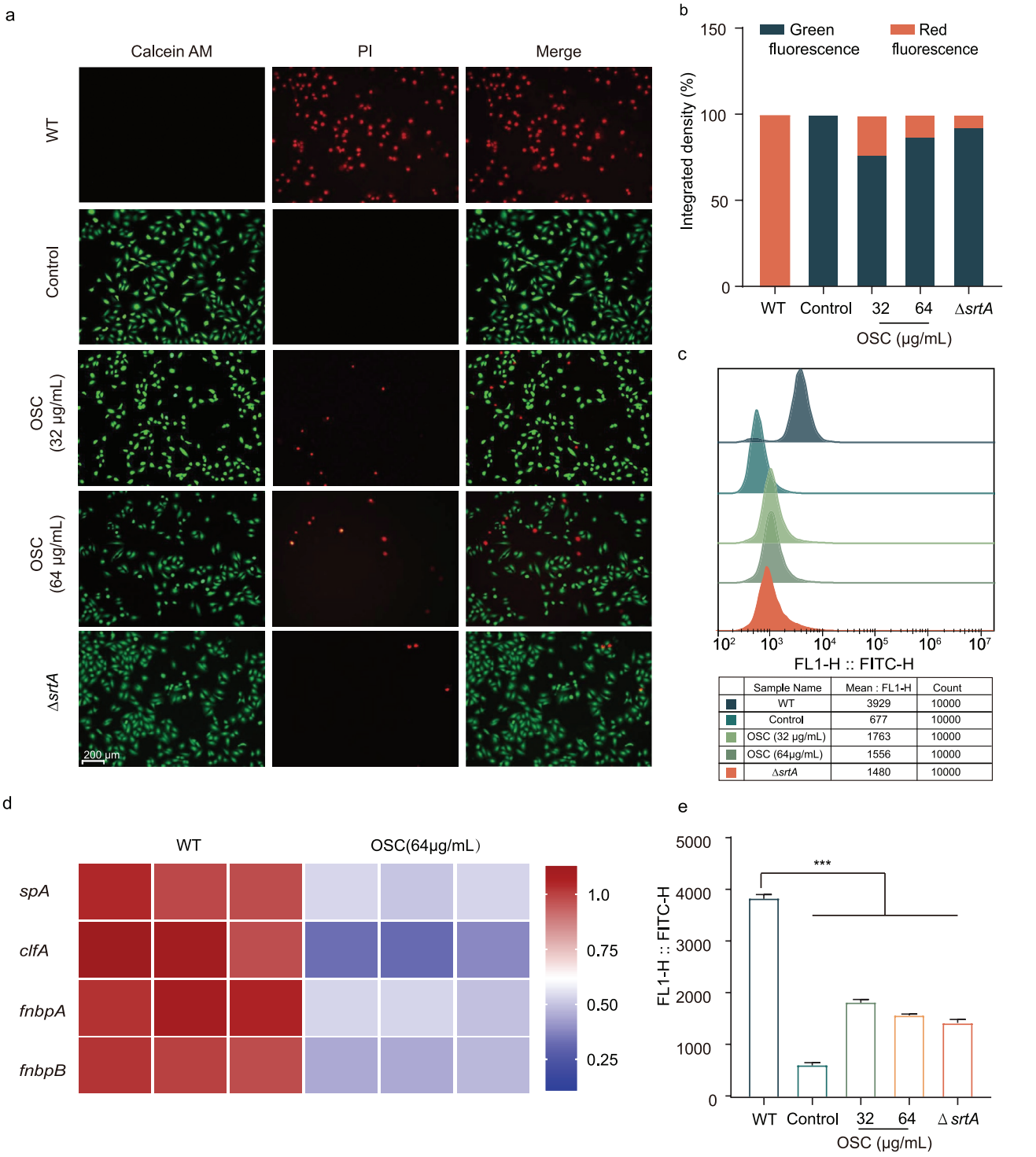

FIGURE 3 | OSC affects the expression of surface virulence factors and inhibits the biological function of SrtA. (a, b) The protective effect of different concentrations of OSC (32–64 μg/mL) on A549 cells infected with *S. aureus* was detected via the calcein AM/PI reagent. Live cells emitted green fluorescence, whereas dead cells emitted red fluorescence, indicating the protective effect of OSC on host cells. A quantitative statistical analysis of red and green fluorescence. (c, e) The effect of OSC on the expression of SpA in *S. aureus* was examined via flow cytometry, which revealed that OSC was able to downregulate the level of SpA. Quantitative analysis of *S. aureus* SpA expression. (d) The transcription levels of the relevant genes, *spA*, *clfA*, *fnbpA* and *fnbpB*, were detected via RT–qPCR at concentrations of 64 μg/mL. The reference gene used for RT–qPCR was *16S RNA*.

levels. The results showed that after OSC treatment, the fluorescence intensity of IgG gradually decreased (Figure 3c), indicating that OSC weakened the ability of SpA to anchor *S. aureus*. This treatment not only reduced bacterial adhesion but also impaired immune evasion.

In this study, the transcription levels of virulence factor genes (*spA*, *clfA*, *fnbpA* and *fnbpB*) that play important roles in the *S. aureus* infection process were detected via RT–qPCR at a concentration of 64 μg/mL. Compared with those in the untreated group, the expression levels of the *spA*, *clfA*, *fnbpA* and *fnbpB*

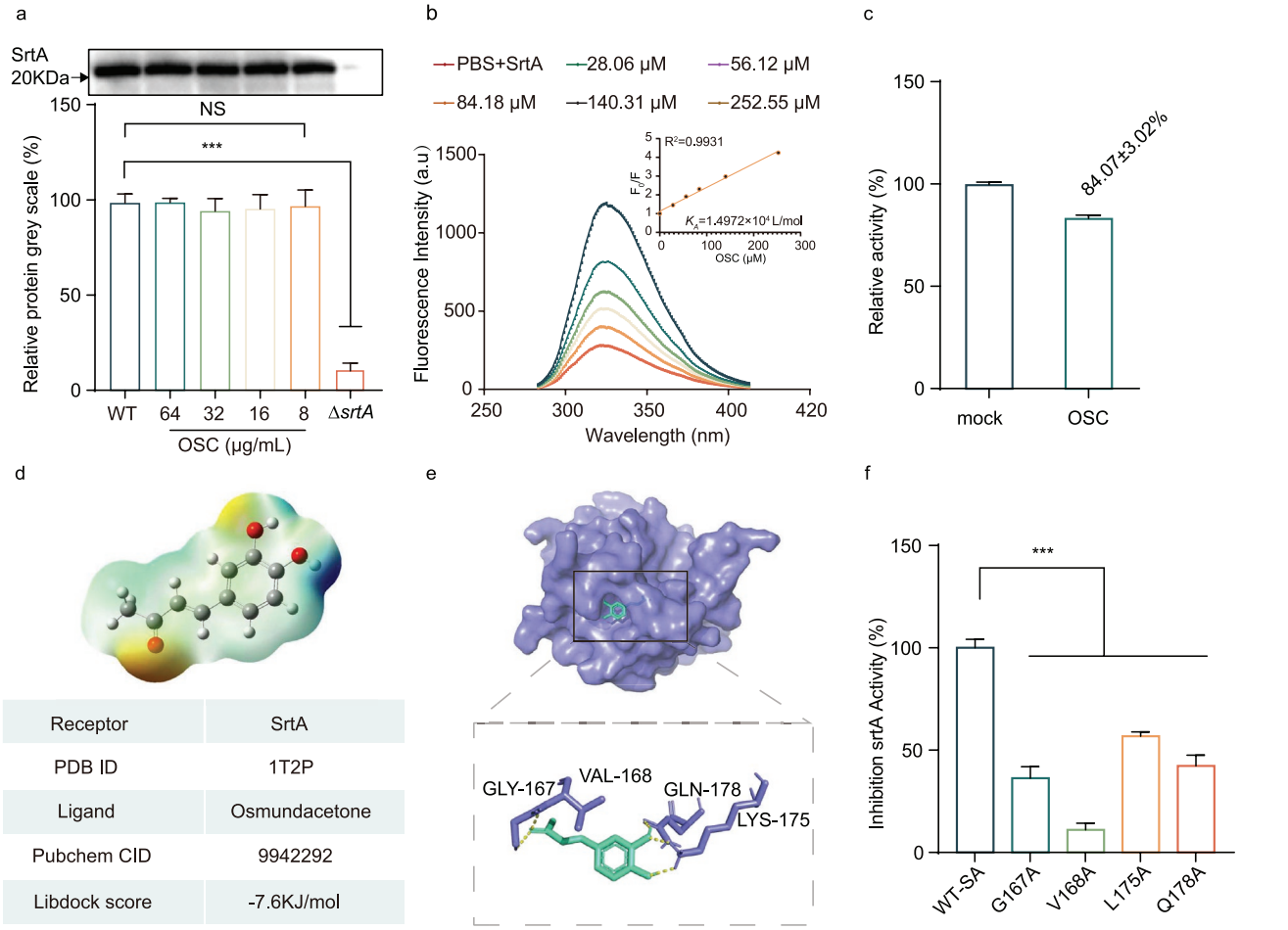

FIGURE 4 | Mechanism of OSC-mediated Inhibition of SrtA, a Virulence Factor in *S. aureus*. (a) Effects of OSC (0–64 μg/mL) on SrtA protein expression were assessed via Western blot, and protein band intensities were quantified using ImageJ software. (b) The interaction between OSC and SrtA was evaluated using the fluorescence quenching method. Fluorescence intensity of SrtA decreased with increasing OSC concentration, suggesting a direct interaction, with a binding constant (K_A) determined by linear regression. (c) SrtA activity was assessed after incubation with buffer or $10\times IC_{50}$ OSC, revealing 84.07% ± 3.02% activity recovery post-OSC treatment. (d) Three-dimensional electrostatic potential mapping of OSC using ABEE, providing insight into OSC-SrtA interactions. (e) Molecular docking analysis of OSC binding to SrtA, illustrating potential molecular interactions. (f) FRET analysis of SrtA activity following coincubation with OSC and SrtA mutants (G167A, V168A, L175A, Q185A). Statistical analysis showed significant differences in activity compared with WT-SrtA ($p < 0.05$), indicating the importance of specific residues for OSC binding. Experiments were repeated three times, and data are presented as mean ± SDs.

genes in USA300 decreased to varying degrees after treatment with 64 μg/mL OSC (Figure 3d).

In conclusion, OSC showed significant efficacy in reducing the pathogenic traits of *S. aureus* (especially MRSA) by inhibiting *S. aureus* adhesion, invasion and biofilm formation processes. Additionally, OSC can inhibit the expression of key virulence genes on the surface of *S. aureus*. These findings highlight the potential of OSC as a cornerstone for novel antimicrobial strategies, providing a foundation for further therapeutic development.

3.3 | Direct Interaction Between OSC and SrtA

In this comprehensive study, we employed biochemical techniques such as western blot analysis and fluorescence quenching assay to explore the intricate effects of OSC on the expression and functionality of the SrtA protein. Western blot analysis robustly demonstrated that varying concentrations of OSC did not markedly alter the expression levels of SrtA (Figure 4a). The band intensity observed in the OSC-treated samples closely paralleled that in the control samples, suggesting that OSC does not directly modulate SrtA expression.

Intriguingly, our subsequent fluorescence quenching experiments revealed a concentration-dependent attenuation of the fluorescence intensity of SrtA, which was correlated with increasing concentrations of OSC. By constructing a Stern–Volmer plot from the linear relationship between F_0/F and the OSC, we determined the binding constant (K_A) to be a substantial 1.49×10^4 L/mol (Figure 4b). This finding underscores a significant molecular interaction between the OSC and SrtA, highlighting the specificity of this interaction.

To further explore the dynamics of this interaction, we conducted a reversible inhibition assay to determine whether the inhibition of SrtA by the OSC could be reversed. After coincubation with a fluorescent substrate peptide at $10\times IC_{50}$ of the

OSC, the SrtA activity substantially recovered to 81.93% ± 1.92% (Figure 4c). This result indicates that the OSC functions as a reversible inhibitor, binding noncovalently to the active site of SrtA and allowing potential therapeutic modulation.

Moreover, molecular docking simulations and electrostatic potential mapping pinpointed GLY-167, VAL-168, GLN-178 and LYS-175 as pivotal binding sites for the interaction of SrtA with OSC (Figure 4e), confirming the biochemical basis of their interaction. The total binding free energy (ΔG_{bind}) of the SrtA–OSC complex was calculated to be −7.6 kcal/mol (Figure 4d).

To validate these findings, we performed FRET assays using wild-type SrtA (WT-SrtA) and several SrtA mutants and assessed their activity in the presence of the OSC via the FRET technique. The diminished SrtA protein activity observed in the G167A and V168A mutants further confirmed that GLY-167 and VAL-168 are critical active sites for the function of SrtA (Figure 4f).

3.4 | Assessment of the Toxicity and Protective Effects of OSC Against *S. aureus* Infection in a *G. mellonella* Model

In this study, we selected *G. mellonella* as a model organism to evaluate the in vivo toxicity and efficacy of a novel antimicrobial agent. The aim of this study was to investigate the toxicity and protective effects of OSC against MRSA infection in *G. mellonella*. Both MRSA and Δ*srtA* were inoculated into *G. mellonella*, and their survival rates, morphological changes, degrees of melanisation and bacterial burdens were monitored over a 96-h period (Figure 5a). The results revealed a significant decrease in the *G. mellonella* survival rate following MRSA infection, dropping to 10% after 12 h, accompanied by a decrease in body colour (Figure 5b), indicating severe infection. However, treatment with OSC (40 mg/kg) significantly increased the survival rate of *G. mellonella* to 50%, which stabilised after 24 h (Figure 5c). Additionally, quantitative analysis of the bacterial load in the hemolymph revealed a significant reduction in the bacterial burden from 8.08 ± 1.0 to 5.72 ± 1.24 lg CFUs/g after OSC treatment (Figure 5d). Compared with the saline control group, the Δ*srtA* group presented similar levels of melanisation, survival rates and bacterial colony counts, further confirming the crucial role of the virulence factor SrtA in *S. aureus* infection. In addition, compared with the WT group, the OSC-treated group (40 mg/kg) presented varying degrees of reduction in appearance, survival curves and bacterial loads, suggesting that OSC effectively reduced the pathogenicity of MRSA.

3.5 | Therapeutic Efficacy of OSC in Treating MRSA-Induced Pneumonia

To further investigate the therapeutic potential of OSC against MRSA infection, a mouse model of MRSA-induced pneumonia was constructed, followed by a series of experimental analyses. The experiments were divided into two dosage groups: a lethal dose group (2×10^8 CFU) and a sublethal dose group (1×10^8 CFU), with intranasal administration (Figure 6a). Survival curve monitoring revealed that the survival rate of the USA300 group in the lethal-dose infection group decreased to 20% within 96 h, confirming the successful establishment of the pneumonia model. In contrast, the Δ*srtA* strain infected with a sublethal dose had a survival rate of 90% at 24 h, which remained stable, indicating that the virulence factor SrtA plays a crucial role in MRSA-induced acute pneumonia (Figure 6b). OSC (40 mg/kg) treatment significantly improved the survival rate of the mice to 60%, demonstrating protective effects against MRSA-induced pneumonia. The bacterial burden in the lungs significantly decreased in the OSC group (Figure 6c), indicating that OSC can reduce MRSA invasion and lung damage. Additionally, the lung W/D weight ratio decreased after OSC treatment (Figure 6d), suggesting an alleviation of pulmonary oedema and tissue damage. In our experiments, the immune cell composition of mouse lung tissue homogenates was analysed by flow cytometry. In particular, we examined the expression levels of the macrophage-specific antigen CD11b and the neutrophil-specific antigen Ly6G. In WT mice, the proportion of both CD11b- and Ly6G-positive cells was significantly greater than 50%, a phenomenon indicative of a significant accumulation of macrophages and neutrophils in the lung tissues of WT mice, which is consistent with the expected pathological changes in the *S. aureus*-induced acute pneumonia model (Figure 6e). Compared with those in the WT group, the proportions of CD11b- and Ly6G-positive cells in the groups treated with different doses of OSC appeared to be reduced to different degrees, indicating that OSC treatment attenuated *S. aureus*-induced inflammatory responses in the lungs. Notably, the degree of lung tissue inflammation in the Δ*srtA* mutant strain mice was similar to that in the control group, highlighting the important role of SrtA in *S. aureus*-induced lung infections and providing further evidence for the anti-inflammatory effects of OSC.

The H&E staining results of the mouse lung tissues are shown in Figure f. In the infection group, extensive infiltration of inflammatory cells was observed in the alveolar walls and interstitial tissues, accompanied by significant thickening of the alveolar walls, alveolar collapse and widening and oedema of the interstitial tissues. In contrast, the lung tissues from the OSC-treated group presented relatively intact alveolar structures, with reduced infiltration of inflammatory cells and alleviated oedema in the interstitial tissue. Compared with those in the OSC-treated group, the lung tissue structure in the vancomycin-treated group was more intact, with well-preserved alveolar morphology, significantly reduced infiltration of inflammatory cells and improved alleviation of lung tissue damage. These results indicate that both vancomycin and OSC play a role in alleviating inflammation and repairing lung tissue damage in mice, although vancomycin has more pronounced therapeutic effects. Immunohistochemical staining revealed a marked reduction in F4/80-positive macrophage expansion (Figure 6g), further supporting the therapeutic potential of OSC in reducing the severity of MRSA-induced pneumonia in mice.

4 | Discussion

The widespread use of antibiotics has resulted in a crisis in global health due to the emergence of drug-resistant bacteria such as MRSA. Recognised by the Infectious Diseases Society

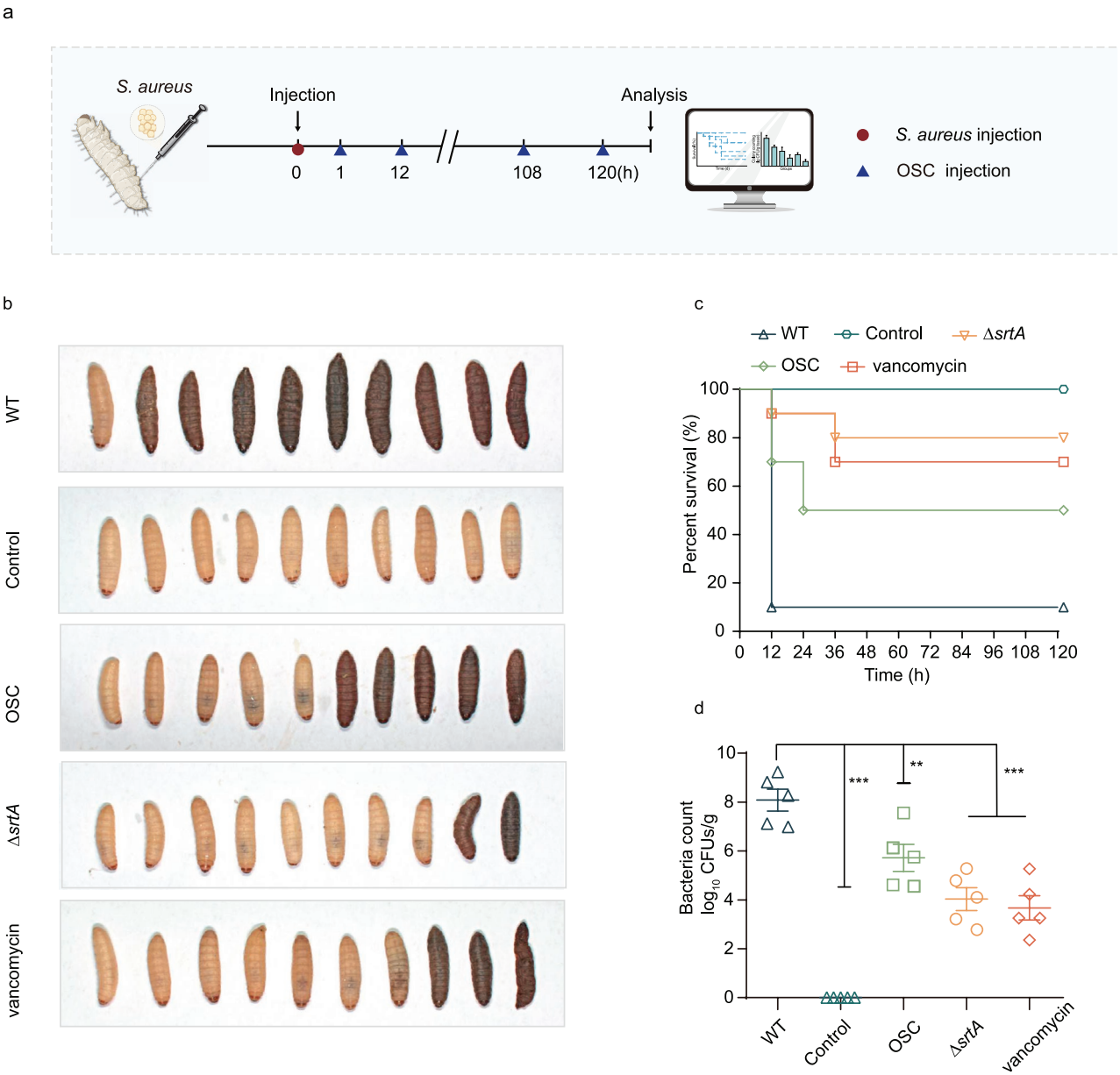

FIGURE 5 | Protective effect of OSC against infections induced by *S. aureus* with *G. mellonella*. (a) Schematic diagram showing the comprehensive evaluation of the protective effect of the compound OSC against *S. aureus* infection in *G. mellonella*. There were five groups, each containing 10 larvae: The WT, control, OSC-treated, Δ*srtA* mutant groups and vancomycin-treated. (b) Effects of different treatments on the survival rate of *S. aureus*-infected *G. mellonella* over a period of 96 h. The degree of mortality of *G. mellonella* was indirectly assessed by observing the degree of blackening of *G. mellonella*. (c) Statistical graph of the effects of different treatments on the survival rate of *S. aureus*-infected *G. mellonella* within 96 h. Differences in survival rates between groups were compared via quantitative analysis. (d) Colony-forming units ($n = 5$) in the body of *G. mellonella* after infection with *S. aureus*, as determined by the agar dilution method.

of America as one of the seven high-priority ESKAPEE (Fymat and Res 2017; Pal et al. 2024) pathogens, MRSA poses a severe threat to healthcare systems worldwide because of its resistance to multiple antibiotics. This situation has prompted a call from the World Health Organization for the development of new strategies to combat these resistant strains (Christaki et al. 2020).

SrtA is a key virulence factor in *S. aureus* that anchors surface proteins to the bacterial cell wall and enhances adherence to host cells, which facilitates infection (Bradshaw et al. 2015; Maresso and Schneewind 2008). The strategy of targeting SrtA for inhibition represents a novel approach in antimicrobial therapy. By focusing on this enzyme, researchers have aimed to reduce the pathogenicity of MRSA without employing traditional bactericidal or bacteriostatic methods (Moldoveanu et al. 2021). This approach could reduce the selective pressure on bacteria, possibly slowing resistance development (Schroeder et al. 2017). Inhibiting SrtA disrupts the expression and function of critical virulence factors in MRSA, thereby diminishing its ability to cause disease (Beceiro et al. 2013).

Phytochemicals derived from plants, including secondary metabolites such as alkaloids (Khan et al. 2021), flavonoids and polyphenols (Ayaz et al. 2019), have gained prominence as effective

antimicrobial agents. These compounds exhibit a wide range of mechanisms, including disruption of cell membranes, inhibition of metabolic pathways, interference with signalling processes and prevention of biofilm formation, thus effectively controlling pathogenic activities (Hancock and Sahl 2006; Silver 2011). They also enhance the host immune response, bolstering resistance to infections (Cushnie et al. 2014). Phytochemicals provide a gentler alternative to traditional antibiotics, offering broad-spectrum

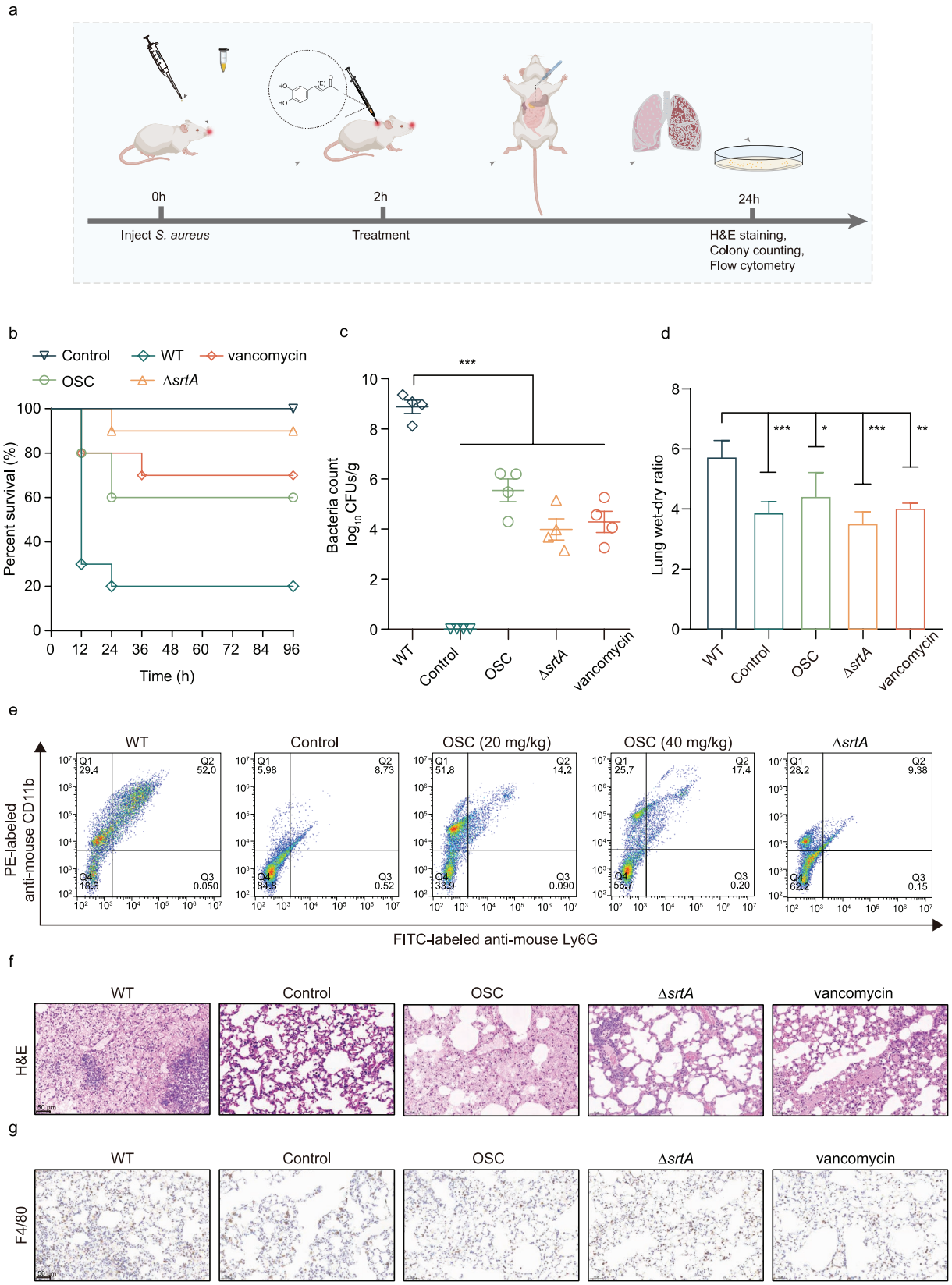

FIGURE 6 | Legend on next page.

FIGURE 6 | In vivo therapeutic effect of OSC on mice with *S. aureus*-induced pneumonia. (a) Experimental flowchart outlining the experimental design and steps of the *S. aureus*-induced pneumonia mouse model. (b) Effects of different treatments on the survival rate of mice with pneumonia over a period of 96 h. The survival rates of the OSC-treated group were compared with those of the control group via observation and recording. (c) Bacterial load of pneumonia-infected mice by the serial dilution method and homogenised lung tissue plate counting. The data are expressed as the means ± SDs, and each group contained six biologically independent animals. (d) Statistical plot of the dry and wet specific gravity of the lung tissue in each group of mice, which was used to assess the extent of pulmonary oedema. (e) The proportions of neutrophils and lymphocytes in the lung tissue of the mice in each group were detected by flow cytometry. FITC-labelled Ly6G and PE-labelled CD11b were used to distinguish and quantify different types of immune cells. (f) Microscopic changes in mouse lung tissues were demonstrated by H&E staining. (g) Microscopic changes in mouse lung tissues were demonstrated by F4/80 staining. Histopathological changes in the lungs of the rats in the OSC (40 mg/kg)-treated group were compared with those in the WT group, and the scale bar represents 50 μm.

antimicrobial activity with reduced toxicity, which makes them an excellent complement to existing antibiotic treatments (Wagner and Ulrich-Merzenich 2009). Additionally, these compounds can synergistically improve the efficacy of traditional antibiotics, lower resistance thresholds and help curb the spread of resistance genes (Rasko and Sperandio 2010).

OSC, a phenolic compound extracted from Osmunda japonica (Zhang et al. 2010), is particularly notable for its antimicrobial properties among phytochemicals. Owing to their extensive pharmacological activities (Lucchini et al. 1990), phenolic compounds, including osmundacetone, exhibit antioxidant, antimicrobial, antiviral (Albano et al. 2016), anti-inflammatory (LI et al. 2019; Wang et al. 2025), anticancer, cardiovascular protective and immunomodulatory effects. Specifically, osmundacetone not only combats pathogens directly but also employs an antivirulence strategy by targeting virulence factors in *S. aureus* rather than merely killing the bacteria. This method significantly lowers the evolutionary pressure on bacteria, presenting a novel direction for antimicrobial therapy that could be essential for managing MRSA infections and potentially other microbial threats.

Current SrtA inhibitors, which include substrate mimetic inhibitors, natural products and synthetic compounds (Cascioferro, et al. 2014) from high-throughput and in silico screenings, have shown promise in reducing the virulence of gram-positive pathogens (Clancy et al. 2010). However, they face limitations, particularly due to the irreversible nature of some compounds, such as pyranoquinone derivatives. These inhibitors form permanent bonds with the active site, leading to potential off-target effects and safety risks (Suree et al. 2009).

OSC, identified through a FRET-based screening assay, exhibits potent inhibitory effects on SrtA at lower concentrations compared to existing inhibitors, demonstrating greater inhibitory potency. A significant advantage of OSC is its reversible mode of action, which potentially reduces safety concerns associated with irreversible inhibitors. This reversible inhibition allows for better control over the drug's activity, minimising unintended interactions and enhancing safety profiles.

Moreover, OSC has shown low cytotoxicity within its effective dosage range, verified by hemolysis and MTT assays. Its low IC_{50} value indicates a strong binding affinity for the SrtA protein at the molecular level with minimal off-target interactions. The use of the SwissADME tool (http://www.swissadme.ch/index.php) confirmed the absence of PAINS motifs in OSC, further supporting its specificity in inhibiting SrtA and preventing the anchoring of surface virulence factors.

One of the key virulence factors anchored by SrtA is SpA, which binds to the Fc region of IgG (Mazmanian et al. 2001). This enables *S. aureus* to evade host immune defences by disrupting antibody-mediated immune responses. Additionally, SpA activates B cells, which in turn lead to immune dysregulation and exacerbation of bacterial infection severity. In this study, we demonstrated that OSC significantly reduced the expression of SpA, which in turn impaired the ability of *S. aureus* to evade host immune defences. This reduction in SpA expression led to decreased bacterial colonisation and dissemination within the host, ultimately attenuating the clinical pathogenicity of the bacteria.

The formation of biofilms is of fundamental importance in the context of infections caused by *S. aureus* (Alharthi et al. 2021; Cascioferro, et al. 2014; Uruén et al. 2020). In the initial phase of biofilm formation, surface proteins such as fibronectin-binding proteins (Fnbps) and Clfs bind to host tissues or medical device surfaces, facilitating the initial adhesion of the biofilm (Bhattacharya et al. 2015). These surface proteins are recognised and anchored by SrtA, thereby promoting bacterial adherence. In the Δ*srtA* mutant strain, the capacity to form biofilms is markedly diminished, resulting in a pronounced reduction in both pathogenicity and antibiotic resistance (Mazmanian et al. 2000). Moreover, RT–qPCR experiments revealed that treatment with OSC resulted in varying degrees of reduction in the expression of biofilm-associated virulence genes, including *clfA* and *fnbpA*. These findings indicate that OSC can disrupt biofilm formation by inhibiting SrtA.

Fluorescence quenching experiments confirmed that the OSC exerts a direct inhibitory effect on SrtA. To gain further insight into the interaction mechanism between OSC and SrtA, we employed molecular modelling techniques to investigate their binding characteristics. The analysis revealed that GLY-167, VAL-168, GLN-178 and LYS-175 are potential binding sites for SrtA and OSC, a finding that was further validated by site-directed mutagenesis. These noncovalent interactions are of paramount importance for the inhibitory activity of OSC. Furthermore, subsequent biological evaluations demonstrated that OSC treatment significantly increased the survival rate of mice infected with lethal doses of MRSA while also reducing the bacterial load and mitigating pathological damage and pulmonary inflammation. The therapeutic effects observed are likely attributable to the ability of OSC to inhibit SrtA, thereby

reducing the adhesion and invasion of *S. aureus* into host lung epithelial cells. The aforementioned mechanism was subsequently validated through invasion assays and live/dead cell assays in A549 cells. These results are consistent with the in vivo data, collectively supporting the conclusion that OSC, by inhibiting SrtA activity, reduces *S. aureus* adhesion and invasion capabilities, thereby protecting host cells and increasing survival rates in the infection model.

As antibiotic resistance becomes increasingly problematic, the development of new anti-infection strategies is critical. This study demonstrates for the first time that OSC effectively inhibits SrtA activity, reducing the pathogenicity of MRSA and establishing its potential as a therapeutic agent for MRSA infections. Future research will focus on enhancing the pharmacological properties and safety of OSC through structural modifications and exploring its applications in the treatment of other related diseases.

Notably, while OSC shows strong potential against MRSA, its efficacy alone does not match that of common antibiotics. Therefore, OSC could serve as a potential adjuvant to traditional antibiotics, helping to reduce the occurrence of resistance when used in combination therapy. This combined treatment approach could enhance the effectiveness of antibiotics and reduce the selective pressure on resistant strains, thereby extending the useful life of antibiotics and offering a more sustainable anti-infection strategy for clinical use.

In summary, this study indicates that OSC, by inhibiting SrtA activity and reducing the pathogenicity of *S. aureus*, provides a promising new avenue for the treatment of MRSA infections. Future work will continue to delve into optimising its pharmacological properties, enhancing its clinical applicability and expanding its potential applications.

Author Contributions

Rong Wang, Chunhui Zhao and Li Wang conceived and designed the study and reviewed and edited the manuscript; Rong Wang and Yueying Wang performed the experiments. Dongbin Guo analysed the data; Xinyao Liu, Yun Sun and Luanbiao Sun participated in designing the study and drafting or revising the manuscript; Li Wang provided funding acquisition; Bingmei Wang supervised the study. All the authors read and approved the manuscript.

Acknowledgements

This work was supported by the Jilin Provincial Science and Technology Development Plan (YDZJ202501ZYTS177; YDZJ202401113ZYTS) and the Jilin Provincial Traditional Chinese Medicine Science and Technology Program (2024069).

Ethics Statement

The animal experiments were approved by the Experimental Animal Ethics Committee of Changchun University of Chinese Medicine, in accordance with guidelines under approval number 2024039.

Conflicts of Interest

The authors declare no conflicts of interest.

Data Availability Statement

The datasets generated during and/or analysed during the current study are available from the corresponding author upon reasonable request.

References

Ahmad-Mansour, N., P. Loubet, C. Pouget, et al. 2021. "*Staphylococcus aureus* Toxins: An Update on Their Pathogenic Properties and Potential Treatments." *Toxins* 13: 677.

Albano, M., F. C. B. Alves, B. F. M. T. Andrade, et al. 2016. "Antibacterial and Anti-*Staphylococcal* Enterotoxin Activities of Phenolic Compounds." *Innovative Food Science & Emerging Technologies* 38: 83–90.

Alharthi, S., S. E. Alavi, P. M. Moyle, and Z. M. Ziora. 2021. "Sortase A (SrtA) Inhibitors as an Alternative Treatment for Superbug Infections." *Drug Discovery Today* 26: 2164–2172.

Askarian, F., S. Uchiyama, J. A. Valderrama, et al. 2017. "Serine-Aspartate Repeat Protein D Increases Virulence and Survival in Blood." *Infection and Immunity* 85: e00559.

Ayaz, M., F. Ullah, A. Sadiq, et al. 2019. "Synergistic Interactions of Phytochemicals With Antimicrobial Agents." *Potential Strategy to Counteract Drug Resistance* 308: 294–303.

Beceiro, A., M. Tomás, and G. Bou. 2013. "Antimicrobial Resistance and Virulence: A Successful or Deleterious Association in the Bacterial World?" *Clinical Microbiology Reviews* 26: 185–230.

Béni, Z., M. Dékány, A. Sárközy, et al. 2021. *Triterpenes and Phenolic Compounds From the Fungus Fuscoporia Torulosa: Isolation*, 26. Structure Determination and Biological Activity.

Bhattacharya, M., D. J. Wozniak, P. Stoodley, and L. Hall-Stoodley. 2015. "Prevention and Treatment of *Staphylococcus aureus* Biofilms." *Expert Review of Anti-Infective Therapy* 13: 1499–1516.

Bradshaw, W. J., A. H. Davies, C. J. Chambers, A. K. Roberts, C. C. Shone, and K. R. Acharya. 2015. "Molecular Features of the Sortase Enzyme Family." *FEBS Journal* 282: 2097–2114.

Cascioferro, S., M. Totsika, and D. Schillaci. 2014a. "Sortase A: An Ideal Target for Anti-Virulence Drug Development." *Microbial Pathogenesis* 77: 105–112.

Cascioferro, S., M. Totsika, and D. Schillaci. 2014b. "Sortase A: An Ideal Target for Anti-Virulence Drug Development." *Microbial Pathogenesis* 77: 105–112.

Chambers, H. F., and F. R. Deleo. 2009. "Waves of Resistance: *Staphylococcus aureus* In the Antibiotic Era." *Nature Reviews Microbiology* 7: 629–641.

Chan, A. H., J. Wereszczynski, B. R. Amer, et al. 2013. "Discovery of *Staphylococcus aureus* Sortase A Inhibitors Using Virtual Screening and the Relaxed Complex Scheme." *Chemical Biology & Drug Design* 82: 418–428.

Cheung, G. Y. C., J. S. Bae, and M. Otto. 2021. "Pathogenicity and Virulence of *Staphylococcus aureus*." *Virulence* 12: 547–569.

Christaki, E., M. Marcou, and A. Tofarides. 2020. "Antimicrobial Resistance in Bacteria: Mechanisms, Evolution, and Persistence." *Journal of Molecular Evolution* 88: 26–40.

Clancy, K. W., J. A. Melvin, and D. G. J. P. S. McCafferty. 2010. "Sortase Transpeptidases: Insights Into Mechanism, Substrate Specificity and Inhibition." *Peptide Science* 94: 385–396.

Cushnie, T. T., B. Cushnie, and A. J. J. I. J. O. A. A. Lamb. 2014. "Alkaloids: An Overview of Their Antibacterial." *Antibiotic-Enhancing and Antivirulence Activities* 44: 377–386.

Deng, F. K., L. Zhang, Y. T. Wang, O. Schneewind, and S. B. Kent. 2014. "Total Chemical Synthesis of the Enzyme Sortase A(ΔN59) With Full

Catalytic Activity." *Angewandte Chemie International Edition in English* 53: 4662–4666.

Enright, M. C., N. P. Day, C. E. Davies, S. J. Peacock, and B. G. Spratt. 2000. "Multilocus Sequence Typing for Characterization of Methicillin-Resistant and Methicillin-Susceptible Clones of *Staphylococcus aureus*." *Journal of Clinical Microbiology* 38: 1008–1015.

Foster, T. J. 2019. "Surface Proteins of *Staphylococcus aureus*." *Microbiology Spectrum* 7: 0046.

Fymat, A. L. J. B. J. S., and T. Res. 2017. "Antibiotics and Antibiotic Resistance." *Biomedical Journal of Scientific and Technical Research* 1: 1–16.

Ganesh, V. K., E. M. Barbu, C. C. Deivanayagam, et al. 2011. "Structural and Biochemical Characterization of *Staphylococcus aureus* Clumping Factor B/Ligand Interactions." *Journal of Biological Chemistry* 286: 25963–25972.

Gao, W., and L. Zhang. 2021. "Nanomaterials Arising Amid Antibiotic Resistance." *Nature Reviews. Microbiology* 19: 5–6.

Gatta, V., T. Tomašič, J. Ilaš, et al. 2020. "A New Cell-Based AI-2-Mediated Quorum Sensing Interference Assay in Screening of LsrK-Targeted Inhibitors." *Chembiochem: A European Journal of Chemical Biology* 21: 1918–1922.

González-García, S., A. Hamdan-Partida, J. J. Valdez-Alarcón, A. Bustos-Hamdan, and J. Bustos-Martínez. 2022. "Main Factors of *Staphylococcus aureus* Associated With the Interaction to the Cells for Their Colonization and Persistence." In *Staphylococcal Infections-Recent Advances and Perspectives*. IntechOpen.

Ha, M. W., S. W. Yi, and S. M. Paek. 2020. "Design and Synthesis of Small Molecules as Potent *Staphylococcus aureus* Sortase A Inhibitors." *Antibiotics (Basel, Switzerland)* 9: 706.

Hancock, R. E., and H. G. Sahl. 2006. "Antimicrobial and Host-Defense Peptides as New Anti-Infective Therapeutic Strategies." *Nature Biotechnology* 24: 1551–1557.

Hanselman, B. A., S. A. Kruth, J. Rousseau, and J. S. Weese. 2009. "Coagulase Positive Staphylococcal Colonization of Humans and Their Household Pets." *Canadian Veterinary Journal* 50: 954–958.

Howden, B. P., S. G. Giulieri, T. Wong Fok Lung, et al. 2023. "*Staphylococcus aureus* Host Interactions and Adaptation." *Nature Reviews. Microbiology* 21: 380–395.

Humphries, R., A. M. Bobenchik, J. A. Hindler, and A. N. Schuetz. 2021. "Overview of Changes to the Clinical and Laboratory Standards Institute Performance Standards for Antimicrobial Susceptibility Testing, M100, 31st Edition." *Journal of Clinical Microbiology* 59: e0021321.

Ito, T., Y. Katayama, and K. Hiramatsu. 1999. "Cloning and Nucleotide Sequence Determination of the Entire Mec DNA of Premethicillin-Resistant *Staphylococcus aureus* N315." *Antimicrobial Agents and Chemotherapy* 43: 1449–1458.

Jenul, C., and A. R. Horswill. 2019. "Regulation of *Staphylococcus aureus* Virulence." *Microbiology Spectrum* 7: 2.

Khan, M. A., A. Khan, M. Azam, et al. 2021. "Liposomal Ellagic Acid Alleviates Cyclophosphamide-Induced Toxicity and Eliminates the Systemic Cryptococcus Neoformans Infection in Leukopenic Mice." *Pharmaceutics* 13: 882.

Kowalska, M., W. Dębek, and E. Matuszczak. 2021. "Infantile Hemangiomas: An Update on Pathogenesis and Treatment." *Journal of Clinical Medicine* 10: 4631.

Lakhundi, S., and K. Zhang. 2018. "Methicillin-Resistant *Staphylococcus aureus*: Molecular Characterization, Evolution, and Epidemiology." *Clinical Microbiology Reviews* 31: e00020-18.

LI, K., Q. Yang, T.-T. Zhou, et al. 2019. "Protective Effect of Phenolic Compound of Osmundae Rhizoma on Systemic Inflammatory Response Syndrome in Mice." Chinese Journal of Experimental Traditional Medical Formulae: 24, 55–60.

Liu, C., A. Bayer, S. E. Cosgrove, et al. 2011. "Clinical Practice Guidelines by the Infectious Diseases Society of America for the Treatment of Methicillin-Resistant *Staphylococcus aureus* Infections in Adults and Children: Executive Summary." *Clinical Infectious Diseases: An Official Publication of the Infectious Diseases Society of America* 52: 285–292.

Lowy, F. D. 1998. "*Staphylococcus aureus* Infections." *New England Journal of Medicine* 339: 520–532.

Lucchini, J. J., J. Corre, and A. Cremieux. 1990. "Antibacterial Activity of Phenolic Compounds and Aromatic Alcohols." *Research in Microbiology* 141: 499–510.

Maresso, A. W., and O. Schneewind. 2008. "Sortase as a Target of Anti-Infective Therapy." *Pharmacological Reviews* 60: 128–141.

Marshall, A. C. 2020. "Traditional Chinese Medicine and Clinical Pharmacology." In *Traditional Chinese Medicine and Clinical Pharmacology*. Springer.

Mazmanian, S. K., G. Liu, E. R. Jensen, E. Lenoy, and O. Schneewind. 2000. "*Staphylococcus aureus* Sortase Mutants Defective in the Display of Surface Proteins and in the Pathogenesis of Animal Infections." *Proceedings of the National Academy of Sciences of the United States of America* 97: 5510–5515.

Mazmanian, S. K., H. Ton-That, and O. Schneewind. 2001. "Sortase-Catalyzed Anchoring of Surface Proteins to the Cell Wall of *Staphylococcus aureus*." *Molecular Microbiology* 40: 1049–1057.

Moldoveanu, A. L., J. A. Rycroft, and S. Helaine. 2021. "Impact of Bacterial Persisters on Their Host." *Current Opinion in Microbiology* 59: 65–71.

Monecke, S., G. Coombs, A. C. Shore, et al. 2011. "A Field Guide to Pandemic, Epidemic and Sporadic Clones of Methicillin-Resistant *Staphylococcus aureus*." *PLoS One* 6: e17936.

Nagarajan, A., K. Scoggin, J. Gupta, et al. 2024. "Collaborative Cross Mice Have Diverse Phenotypic Responses to Infection With Methicillin-Resistant *Staphylococcus aureus* USA300." *PLoS Genetics* 20: e1011229.

Nisar, S., L. D. Kirkpatrick, and J. W. Shupp. 2021. "Bacterial Virulence Factors and Their Contribution to Pathophysiology After Thermal Injury." *Surgical Infections* 22: 69–76.

Pal, N., P. Sharma, M. Kumawat, et al. 2024. "Phage Therapy: An Alternative Treatment Modality for MDR Bacterial Infections." *Infectious Diseases* 56: 785–817.

Pan, Y., J. Zeng, L. Li, et al. 2020. "Coexistence of Antibiotic Resistance Genes and Virulence Factors Deciphered by Large-Scale Complete Genome Analysis." *mSystems* 5: e00821-19.

Papadopoulou, A., R. J. Green, and R. A. Frazier. 2005. "Interaction of Flavonoids With Bovine Serum Albumin: A Fluorescence Quenching Study." *Journal of Agricultural and Food Chemistry* 53: 158–163.

Rasko, D. A., and V. J. N. R. D. D. Sperandio. 2010. "Anti-Virulence Strategies to Combat Bacteria-Mediated Disease." *Nature Reviews. Drug Discovery* 9: 117–128.

Rio, D. C., M. Ares, G. J. Hannon, and T. W. Nilsen. 2010. "Purification of RNA Using TRIzol (TRI Reagent)." *Cold Spring Harbor Protocols* 2010: pdb.prot5439.

Schroeder, M., B. D. Brooks, and A. E. Brooks. 2017. "The Complex Relationship Between Virulence and Antibiotic Resistance." *Genes* 8: 10039.

Silver, L. L. J. C. M. R. 2011. "Clinical Microbiology Reviews." *Challenges of Antibacterial Discovery* 24: 71–109.

Song, W., B. Wang, L. Sui, et al. 2022. "Tamarixetin Attenuated the Virulence of *Staphylococcus aureus* by Directly Targeting Caseinolytic Protease P." *Journal of Natural Products* 85: 1936–1944.

Suree, N., C. K. Liew, V. A. Villareal, et al. 2009. "The Structure of the Staphtlococcus Aureus Sortase-Substrate Complex Reveals How the Universally Conserved LPXTG Sorting Signal Is Recognized." *Journal of Biological Chemistry* 284: 24465–24477.

Tilouche, L., R. Ben Dhia, S. Boughattas, et al. 2021. "*Staphylococcus aureus* Ventilator-Associated Pneumonia: A Study of Bacterio-Epidemiological Profile and Virulence Factors." *Current Microbiology* 78: 2556–2562.

Tong, S. Y., J. S. Davis, E. Eichenberger, T. L. Holland, and V. G. Fowler. 2015. "*Staphylococcus aureus* Infections: Epidemiology, Pathophysiology, Clinical Manifestations, and Management." *Clinical Microbiology Reviews* 28: 603–661.

Trinh, T. A., Y. H. Seo, S. Choi, J. Lee, and K. S. J. B. Kang. 2021. "Protective Effect of Osmundacetone Against Neurological Cell Death Caused by Oxidative Glutamate Toxicity." *Biomolecules* 11: 328.

Turner, N. A., B. K. Sharma-Kuinkel, S. A. Maskarinec, et al. 2019. "Methicillin-Resistant *Staphylococcus aureus*: An Overview of Basic and Clinical Research." *Nature Reviews. Microbiology* 17: 203–218.

Uruén, C., G. Chopo-Escuin, J. Tommassen, R. C. Mainar-Jaime, and J. Arenas. 2020. "Biofilms as Promoters of Bacterial Antibiotic Resistance and Tolerance." *Antibiotics (Basel, Switzerland)* 10: 10003.

Wagner, H., and G. J. P. Ulrich-Merzenich. 2009. "Synergy Research: Approaching a New Generation of Phytopharmaceuticals." *Phytomedicine* 16: 97–110.

Wallock-Richards, D. J., J. Marles-Wright, D. J. Clarke, et al. 2015. "Molecular Basis of *Streptococcus mutans* Sortase A Inhibition by the Flavonoid Natural Product Trans-Chalcone." *Chemical Communications (Cambridge, England)* 51: 10483–10485.

Wang, Z., Y. Liu, C. Feng, et al. 2025. "The Therapeutic Potential of Osmundacetone for Rheumatoid Arthritis: Effects and Mechanisms on Osteoclastogenesis." *European Journal of Pharmacology* 987: 177135.

Weiss, W. J., E. Lenoy, T. Murphy, et al. 2004. "Effect of Srta and Srtb Gene Expression on the Virulence of *Staphylococcus aureus* in Animal Models of Infection." *Journal of Antimicrobial Chemotherapy* 53: 480–486.

Wertheim, H. F., D. C. Melles, M. C. Vos, et al. 2005. "The Role of Nasal Carriage in *Staphylococcus aureus* Infections." *Lancet Infectious Diseases* 5: 751–762.

Wilson, J., R. Guy, S. Elgohari, et al. 2011. "Trends in Sources of Meticillin-Resistant *Staphylococcus aureus* (MRSA) Bacteraemia: Data From the National Mandatory Surveillance of MRSA Bacteraemia in England, 2006-2009." *Journal of Hospital Infection* 79: 211–217.

Xiang, H., F. Cao, D. Ming, et al. 2017. "Aloe-Emodin Inhibits *Staphylococcus aureus* Biofilms and Extracellular Protein Production at the Initial Adhesion Stage of Biofilm Development." *Applied Microbiology and Biotechnology* 101: 6671–6681.

Xiang, H., Y. Feng, J. Wang, et al. 2012. "Crystal Structures Reveal the Multiligand Binding Mechanism of *Staphylococcus aureus* ClfB." *PLoS Pathogens* 8: e1002751.

Yarovoy, J. Y., A. A. Monte, B. C. Knepper, and H. L. Young. 2019. "Epidemiology of Community-Onset *Staphylococcus aureus* Bacteremia." *Western Journal of Emergency Medicine* 20: 438–442.

Zecconi, A., and F. Scali. 2013. "*Staphylococcus aureus* Virulence Factors in Evasion From Innate Immune Defenses in Human and Animal Diseases." *Immunology Letters* 150: 12–22.

Zhang, D., B. Li, L. Yang, M. Fu, and J. J. C. P. J. Fang. 2010. "Isolation and Determination of Osmundacetone in Osmundae Rhizoma." *Journal of Chinese Pharmaceutical Sciences* 45: 1612–1614.

Zhu, Y.-P., and H. J. Woerdenbag. 1995. "Traditional Chinese Herbal Medicine." *Science* 17: 103–112.

Supporting Information

Additional supporting information can be found online in the Supporting Information section.